ENHANCED TURBULENCE MODELING IN FloEFD™

WHITEPAPER

Mentor Graphics®

MECHANICAL ANALYSIS

www.mentor.com

CONTENTS

INTRODUCTION

Today, product lifecycle management concepts (PLM) are widely deployed by engineers in many industries as the means by which 3D manufactured product data are used and maintained consistently during an entire product's lifecycle and across all its design changes. The basis of a PLM concept is the availability of high-quality, complete, detailed, and accurate 3D product model data within a CAD system as the central element. 3D product model data are therefore both the foundation and starting point for all virtual prototyping and physical simulations today. The use of fluid flow simulations (or Computational Fluid Dynamics, CFD) in such a CAD-embedded context is obviously very attractive as it can not only accelerate the design process, but it can make these processes more predictable and reliable, against a background of increasing design complexity and dependence on external development partners.

The systematic search for the best solution for a design is the objective of most CFD simulations and CFD software packages. The main criterion for flow and heat transfer simulation as an integral part of a PLM concept is efficient turnaround of high quality CFD solutions, from geometry changes to resultant engineering interpretation in order to keep pace with design changes. To make CFD usable for mechanical designers and design engineers from other engineering disciplines, the FloEFD product from Mentor Graphics is a unique CAD-embedded general purpose concurrent CFD software package largely automated to minimize the specialist expertise required to operate traditional CFD software. The capabilities required for CAD-embedded CFD to not only handle very complex geometries without simplification, but also to simulate complex industrial turbulent flows with heat and mass transfer is very important together with benchmarking FloEFD's turbulence capabilities against some classic industrial CFD validation cases. FloEFD is a mature code with over 10 years of commercial presence and a thousand man-years of development effort behind it (see Gavriliouk 1993). It utilizes both a modified k-ε two-equation turbulence model designed to simulate accurately a wide range of turbulence scenarios in association with its pioneering immersed boundary Cartesian meshing techniques that allow for accurate flow field resolution with low cell mesh densities (see Mentor Graphics Corp. 2011). For more information on immersed boundary meshes see for instance Kalitzin and Iaccarino (2002) and their work at Stanford University with General Motors on this approach for generating fast turnaround times for CFD simulations in upfront engineering design studies.

Depending on the fluid being examined and the flow conditions being considered any fluid flow situation can be viewed (Schlichting, 1959) as either:

- Laminar (a smooth flow without any disturbances), or
- Turbulent (a flow regime characterized by random three-dimensional vorticity and intensive mixing), or
- Transitional between laminar and turbulent (an alternation between laminar and turbulent flow regions).

There are usually no difficulties involved with CFD codes in simulating laminar flows which have clear unique solutions. However, direct simulations of turbulent flows taking into account fluid volume fluctuations are practically impossible for industrial situations because of the small physical sizes involved and the wide spectra of velocity fluctuations that would require extremely fine computation meshes to resolve them, long CPU times to simulate them and large computer memory to store the data produced. Hence, industrial turbulent fluid flows are simulated today usually by considering their effect on the time-average fluid flow characteristics in the volume being considered via semi-empirical models of turbulence that close the fundamental Navier-Stokes equations being solved (Wilcox, 1994). The classical two-equation k-ε empirical model for simulating turbulence effects in fluid flow CFD simulation (Launder & Spalding, 1972 and Wilcox, 1994) is still widely used and considered reliable for most industrial CFD simulations and it requires the minimum amount of additional information to calculate the flow field. In FloEFD the k-ε model is used with a range of additional empirical enhancements added to cover a wide range of industrial turbulent flow scenarios (such as shear flows, rotational flows etc.). For instance, damping functions proposed by Lam and Bremhorst (1981) for better boundary layer profile fit when resolving boundary layers with computational meshes have been added (the LB k-ε model).

In addition to turbulence modeling, when simulating flows it is also necessary to simulate fluid boundary layer effects near solid bodies or walls that can be difficult to resolve due to high velocity and temperature gradients across these near-wall layers. To solve the Navier-Stokes equations with a two-equation k-ε turbulence model without resolving the near-wall fluid boundary layer would require a very fine computational mesh, hence a "wall function" approach had been proposed by Launder and Spalding (1972, 1974) to reduce mesh sizes. According to this now classical approach, the fluid wall frictional resistance and heat fluxes from the fluid to the wall are used to calculate the wall boundary conditions for solving the Navier-Stokes equations. Naturally, the main domain flow's physical properties will be those of the boundary layer's external boundary conditions.

In FloEFD Van Driest's (1956) universal profiles are employed to describe turbulent boundary layers and two approaches (called "Two-Scale Wall Functions", 2SWF) have been devised to fit a fluid's boundary layer profile relative to the main flow's properties:

1. When the fluid mass centers of the near-wall mesh cells are located inside the boundary layer, i.e. the physical fluid flow boundary layer is thick,
2. When the fluid mass centers of the near-wall mesh cells are located outside the boundary layer, i.e. the physical fluid flow boundary layer is thin.

These two approaches allow FloEFD to overcome the traditional CFD code restriction of having to employ a very fine mesh density near the walls in the calculation domain and to use immersed boundary Cartesian meshes for all geometries (Kalitzin and Iaccarino, 2002).

Both the aforementioned FloEFD modification to the classical k-ε turbulence model and the FloEFD modifications to the Launder-Spalding wall function approach for specifying the wall boundary conditions for the Navier-Stokes equations Mentor Graphics calls "Enhanced Turbulence Modeling" (ETM). Its structure is shown schematically in Fig.1.

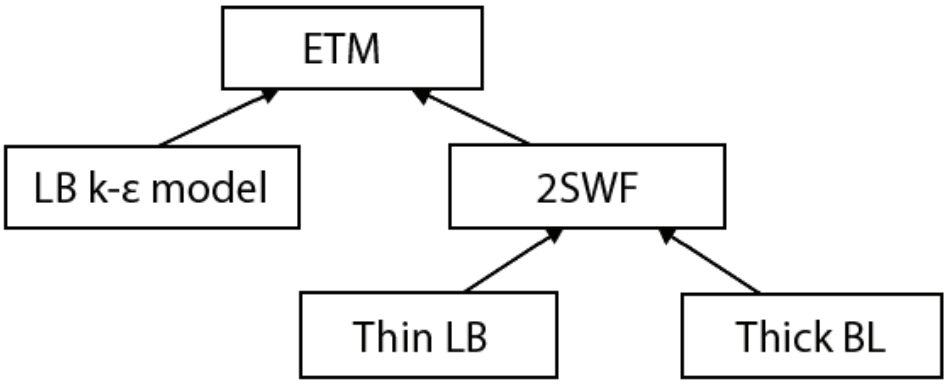

Fig.1. Structure of the ETM approach used in the FloEFD CFD software.

1. THE FLOEFD MODIFIED K-ε TURBULENCE MODEL

The modified k-ε turbulence model with damping functions proposed by Lam and Bremhorst (1981) describes laminar, turbulent, and transitional flows of homogeneous fluids consisting of the following turbulence conservation laws:

$$\frac{\partial \rho k}{\partial t}+\frac{\partial \rho k u_i}{\partial x_i}=\frac{\partial}{\partial x_i}\left[\left(\mu+\frac{\mu_t}{\sigma_k}\right)\frac{\partial k}{\partial x_i}\right]+\tau_{ij}^R\frac{\partial u_i}{\partial x_j}-\rho\varepsilon+\mu_t P_B\,, \tag{1.1}$$

$$\frac{\partial \rho \varepsilon}{\partial t}+\frac{\partial \rho \varepsilon u_i}{\partial x_i}=\frac{\partial}{\partial x_i}\left[\left(\mu+\frac{\mu_t}{\sigma_\varepsilon}\right)\frac{\partial \varepsilon}{\partial x_i}\right]+C_{\varepsilon 1}\frac{\varepsilon}{k}\left[f_1\tau_{ij}^R\frac{\partial u_i}{\partial x_j}+C_B\mu_t P_B\right]-f_2 C_{\varepsilon 2}\frac{\rho\varepsilon^2}{k}\,, \tag{1.2}$$

$$\tau_{ij}=\mu\, s_{ij}\,,\quad \tau_{ij}^R=\mu_t\, s_{ij}-\frac{2}{3}\rho k\delta_{ij}\,,\quad s_{ij}=\frac{\partial u_i}{\partial x_j}+\frac{\partial u_j}{\partial x_i}-\frac{2}{3}\delta_{ij}\frac{\partial u_k}{\partial x_k}\,, \tag{1.3}$$

$$P_B=-\frac{g_i}{\sigma_B}\frac{1}{\rho}\frac{\partial \rho}{\partial x_i}\,, \tag{1.4}$$

where $C_\mu=0.09$, $C_{\varepsilon 1}=1.44$, $C_{\varepsilon 2}=1.92$, $\sigma_k=1$, $\sigma_\varepsilon=1.3$, $\sigma_B=0.9$, $C_B=1$

if $P_B>0$, $C_B=0$ if $P_B<0$. The turbulent viscosity is determined from:

$$\mu_t=f_\mu\cdot\frac{c_\mu\rho k^2}{\varepsilon}\,, \tag{1.5}$$

Lam and Bremhorst´s damping function f_μ is determined from:

$$f_\mu=(1-e^{-0.025R_y})^2\cdot\left[1+\frac{20.5}{R_t}\right], \tag{1.6}$$

where

$$R_y=\frac{\rho\sqrt{ky}}{\mu}\,, \tag{1.7}$$

$$R_t=\frac{\rho k^2}{\mu\varepsilon}\,, \tag{1.8}$$

y is the distance from point to the wall and Lam and Bremhorst's damping functions f_1 and f_2 are determined from:

$$f_1=1+\left[\frac{0.05}{f_\mu}\right]^3\,,\quad f_2=1-e^{R_t^2}\,. \tag{1.9}$$

Lam and Bremhorst's damping functions f_μ, f_1, f_2 decrease turbulent viscosity and turbulence energy and increase the turbulence dissipation rate when the Reynolds number R_y based on the average velocity of fluctuations and distance from the wall becomes too small. When f_μ=1, f_1=1, f_2=1 the approach obtains the original k-ε model.

2. TWO-SCALE WALL FUNCTIONS

The Two-Sales Wall Functions (2SWF) in FloEFD consist of two approaches to coupling the boundary layer calculation with the main flow properties:

1. The thick-boundary-layer approach when $\delta > \mathrm{A} \cdot y$,
2. The thin-boundary-layer approach when $\delta \leq \mathrm{A} \cdot y$,

…where δ is the boundary layer thickness, y is the distance from the near-wall computational mesh cell's fluid mass center to the wall (Fig.2), and $\mathrm{A} \geq 1$ is a coefficient depending on flow conditions.

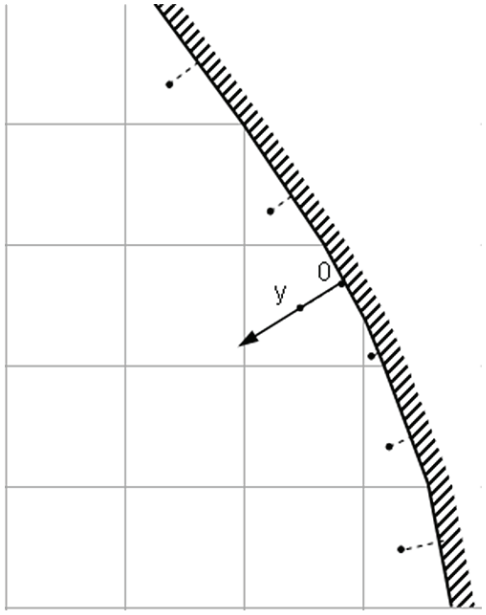

Fig.2. Computational mesh cells near a wall, their fluid mass centers, and the distances from them to the wall (dashed lines)

2.1 THE THICK-BOUNDARY-LAYER APPROACH

When a fluid's boundary layer thickness, $\delta > \mathrm{A} \cdot y$, where *y* is the distance from the near-wall computational mesh cell's fluid mass center to the wall (Fig.2), and $\mathrm{A} \geq 1$ is a coefficient depending on flow conditions, that is, the near-wall computational mesh cell's fluid mass center is located inside the boundary layer. Instead of y, FloEFD uses the dimensionless value, $y^+ = \frac{\sqrt{p\tau_w}\, y}{\mu}$. Since the computational mesh used in FloEFD is always an immersive boundary non-body-fitted Cartesian mesh, y^+ of some near-wall cells could be very small (Fig.2). Hence, the corresponding dimensionless distance from the turbulent equilibrium region's outer boundary to the wall follows from an analysis of the experimental data presented by Wilcox (1994) and is equal to $y^+_{UP} = 300$. With this approach FloEFD obtains the momentum, heat flux, and turbulent boundary conditions for the Navier-Stokes equations which are described below.

2.1.1 THE MOMENTUM BOUNDARY CONDITION

Since $y^+ < y^+_{UP}$, and proceeding from the Van Driest mixing length (1956), the dimensionless longitudinal velocity $u^+ = \frac{u}{\sqrt{\frac{\tau_w}{p}}}$ in the boundary layer depends on the dimensionless y^+ in the following manner:

$$u^+ = \int_0^{y^+} \frac{2 \cdot d\eta}{1 + \sqrt{1 + 4 \cdot \kappa^2 \cdot \eta^2 \cdot \left[1 - \exp\left(-\frac{\eta}{A_v}\right)\right]^2}} \tag{2.1}$$

where $\kappa = 0.4054$ is the Karman constant, $A_v = 26$ is the Van Driest coefficient.

The wall shear stress being the momentum boundary condition governing the fluid velocity u at the near-wall computational mesh cell's center is determined as:

$$\tau_w = \frac{\mu \cdot u}{y} \cdot K\,, \tag{2.2}$$

where $K = K(y^+)$ is a correction coefficient determined from Eq.(2.1) and the function $u^+ = u^+(K(y^+))$.

In FloEFD an equivalent sand wall roughness k_s is taking into account by adding $u^+_{def}(k^+_s)$ function in Eq.(2.1):

$$u^+ = u^+_{def} + \int_0^{y^+} \frac{2 \cdot d\eta}{1 + \sqrt{1 + 4 \cdot \kappa^2 \cdot \eta^2 \cdot \left[1 - \exp\left(-\frac{\eta}{A_v}\right)\right]^2}} \tag{2.3}$$

where u^+_{def} is a dimensionless function of the dimensionless roughness height $k^+_s = \frac{\sqrt{\rho \tau_w}\, k_s}{\mu}$ where k_s is the physical roughness height. The $u^+_{def}(k^+_s)$ function has been determined from the experimental data obtained in flow over a flat plate (Wilcox, 1994) and the boundary condition $u^+_{def}(k_s = 0) = 0$. Correspondingly, $K = K(y^+, k_s^+)$.

If $\mathrm{Re}_\delta = \frac{\rho u^e \delta}{\mu} < 4000$, where u^e is the fluid flow velocity at the boundary layer's fluid boundary, i.e. at the distance of the boundary layer thickness δ from the wall, the boundary layer is considered to be laminar, so $K = 1$.

2.1.2 THE HEAT FLUX BOUNDARY CONDITION

The heat flux across the boundary layer can be determined from:

$$q = C_p \left[\frac{\mu}{\mathrm{Pr}} + \frac{\mu_t}{\mathrm{Pr}_t}\right] \frac{\partial T}{\partial y}\,. \tag{2.4}$$

Since it is constant along the y direction, the heat flux from the fluid to the wall is the heat transfer boundary condition governing the fluid temperature T at the near-wall computational mesh cell's center and it can be determined from:

$$q_w = \lambda \frac{T - T_w}{y} \cdot K \cdot \Phi\,, \tag{2.5}$$

where K is described in the previous Section, and $\Phi = \Phi\left[y^+, \frac{\mathrm{Pr}}{\mathrm{Pr}_t}\right]$ is determined from Eq.(2.4).

In the same manner as in the previous Section, if $\mathrm{Re}_{\delta'} < 4000$ the boundary layer is considered to be laminar, so $K = 1, \Phi = 1$.

2.1.3 TURBULENCE BOUNDARY CONDITIONS

The turbulence boundary conditions for k and ε depend on where the near-wall computational mesh cell's fluid mass center is located: in the turbulence equilibrium region or nearer to the wall. If it is located in the turbulence equilibrium region, i.e. $y^+ > 30$, then at the near-wall computational mesh cell's fluid mass center:

$$\frac{\partial k}{\partial y} = 0\,, \quad \varepsilon = \frac{C_\mu^{0.75} k^{1.5}}{\kappa y} \tag{2.6}$$

If $y^+ \le 30$, i.e. the near-wall computational mesh cell's fluid mass center is located in the turbulence non-equilibrium region, then at this cell's fluid mass center:

$$k^+ = k^+(y^+)\,, \quad \varepsilon^+ = \varepsilon^+(y^+) \tag{2.7}$$

which had been determined from experimental data obtained on a plate (Lapin 1982).

2.2 THE THIN-BOUNDARY-LAYER APPROACH

In the thin-boundary-layer approach the Prandtl boundary layer equations already integrated along the normal to the wall (i.e. along the y ordinate) from 0 (at the wall) to the boundary layer thickness δ are solved along a fluid streamline near the wall. If the boundary layer is laminar these equations are solved in FloEFD with a method of successive approximations based on the Shvetz trial functions technology (Ginzburg 1970). If the boundary layer is turbulent or transitional (between laminar and turbulent), FloEFD uses a generalization of this method to such boundary layers employing the Van Driest hypothesis about the mixing length in turbulent boundary layers (1956).

Three-dimensional effects of fluid flow over concave and convex surface walls, i.e. fluid spilling or collecting near such walls, are taken into account inside FloEFD through corresponding corrections for the wall curvature. Flow and boundary layer separations are also determined with a special method in FloEFD taking the near-zero wall shear stress into account. The equivalent sand wall roughness and the external flow's turbulence on the boundary layer are taken into account through semi-empirical coefficients correcting the wall shear stress and the heat flux from the fluid to the wall in FloEFD. Fluid compressibility, turbulence kinetic energy dissipation, and various mass forces are also taken into account through corresponding empirical and semi-empirical models.

From the boundary layer calculation FloEFD obtains the boundary layer thickness δ, the wall shear stress τ_w^e, and the heat flux from the fluid to the wall q_w^e, which are used as boundary conditions for the Navier-Stokes equations, which are described below.

2.2.4 THE MOMENTUM AND HEAT FLUX BOUNDARY CONDITIONS

The momentum and heat flux boundary conditions are written as

$$\tau_w = \tau_w^e\,, \quad q_w = q_w^e\,, \tag{2.8}$$

2.2.5 THE TURBULENCE BOUNDARY CONDITIONS

Turbulence boundary conditions for k and ε are determined from the condition of turbulence equilibrium in the near-wall computational mesh cell:

$$\frac{\partial k}{\partial y} = 0\,, \quad \varepsilon = \frac{C_\mu^{0.75} k^{1.5}}{\kappa y}\,. \tag{2.9}$$

3. BENCHMARK CFD TURBULENCE VALIDATIONS WITH FLOEFD

Several classical CFD turbulence benchmark examples are presented here to demonstrate:

- FloEFD's accuracy in calculating a wide region of Reynolds number on the immersed boundary Cartesian computational meshes used in FloEFD,
- FloEFD simulation results with refinement of the immersed boundary computational mesh.

3.1 FLOW OVER A FLAT PLATE

Consider an air flow of u_∞=20 m/s velocity over a smooth flat plate of 0.5 m length (Fig.3).

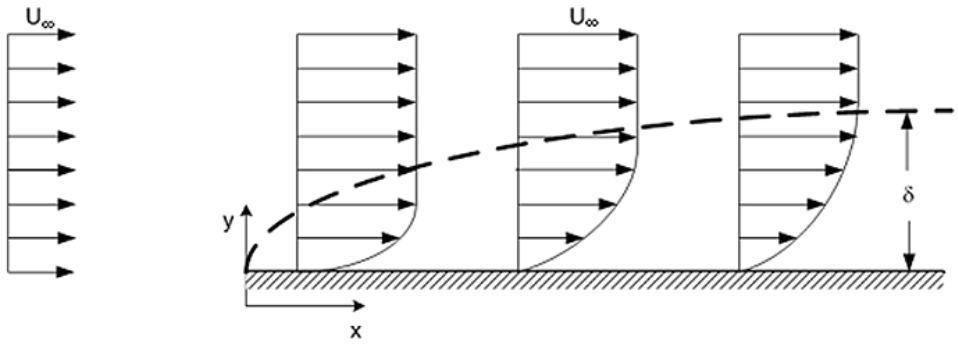

Fig.3. Schematic Representation of boundary layer development on a flat plate.

FloEFD predictions for a computational mesh of 200×50 cells of the obtained fluid velocity field are shown in Fig.4.

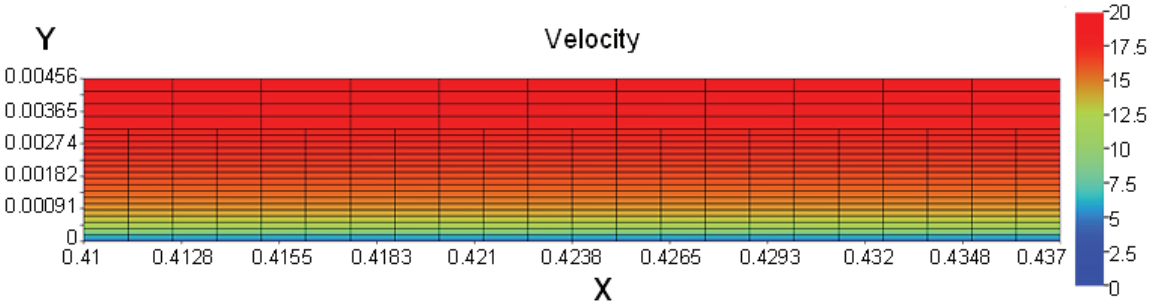

Fig.4. Computational mesh and the resultant velocity distribution at z=0 (zoom-view).

CFD simulation results obtained in FloEFD on a similar computational mesh of 200×100 cells with a varying incoming flow's turbulence intensities of Tu=0.5%, 0.8%, 1.0%, 1.25%, 1.5%, 2.0% are presented in Figs. 5, 6, and 7. In these calculations $y^+ \approx 6$ in the turbulent region, so the boundary layer's laminar sublayer is not being resolved by the computational mesh.

Taking the FloEFD-calculated local flat plate friction coefficient:

$$C_f = \frac{\tau_w}{0.5\rho u_\infty^2} \quad (4.1)$$

for these cases and plotting it versus the Reynolds number $\mathrm{Re}_x = \frac{\rho u_\infty x}{\mu}$ in comparison with the Blasius semi-empirical law (Schlichting 1979) for the laminar boundary layer (on the plate's inlet section):

$$C_f = \frac{0.664}{\sqrt{\mathrm{Re}_x}} \quad (4.2)$$

and the Prandtl-Schlichting semi-empirical law (Schlichting, 1979) for the turbulent boundary layer (on the plate's following section).

$$C_f = (2\lg\mathrm{Re}_x - 0.65)^{-2.3} \quad (4.3)$$

The results are presented in Fig.5:

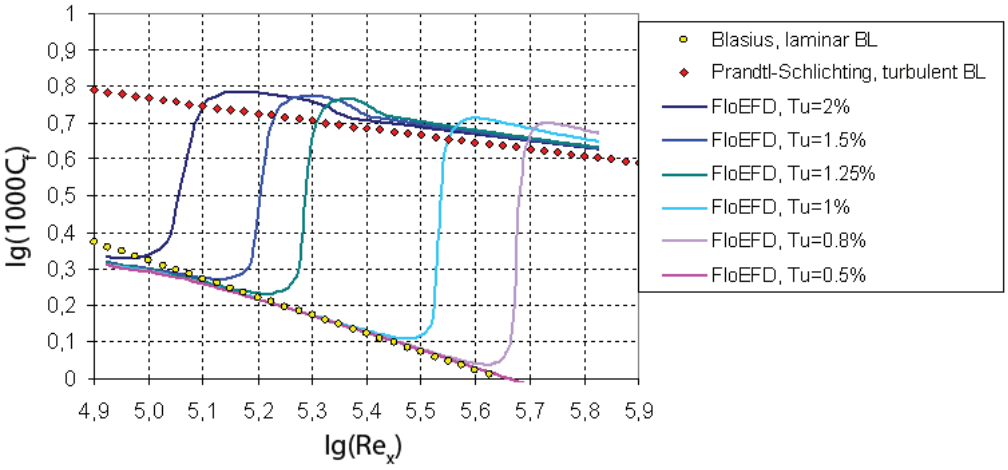

Fig.5. The smooth flat plate's local friction coefficient calculated with FloEFD and for comparison with the Blasius and Prandtl-Schlichting formulae (Schlichting 1979).

In the FloEFD calculations the minimum $\mathrm{Re}_{x'}$ at which the boundary layer is laminar for any incoming flow turbulence intensity, is close to the experimental value of $\mathrm{Re}_x = 6 \cdot 10^4$ (Schlichting, 1979), and the FloEFD-calculated maximum $\mathrm{Re}_{x'}$ at which the boundary layer is turbulent at any incoming flow turbulence intensity, is close to the experimental value of $\mathrm{Re}_x = 3 \cdot 10^6$ (Schlichting, 1979).

A comparison of the FloEFD-calculated dimensionless longitudinal velocity profile, $u^+ = u^+(\ln y^+)$, at the plate inlet and exit sections with the experimental data in Wilcox (1994) and the semi-empirical linear profile of the dimensionless longitudinal velocity in laminar boundary layers (Schlichting, 1979) and the semi-empirical logarithmic profile of the dimensionless longitudinal velocity in turbulent boundary layers is made in Fig.6.

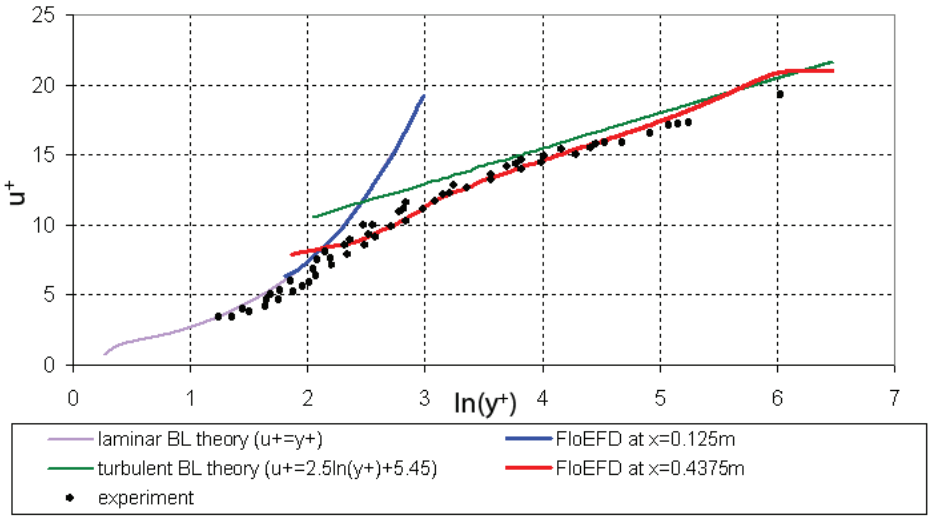

Fig.6. The flat plate boundary layer velocity profiles calculated with FloEFD on the flat plate inlet section with laminar boundary layer (x=0,125m), on the flat plate exit section with turbulent boundary layer (x=0,4375m) in comparison with experimental data (Ref.2) and semi-empirical theory (Schlichting, 1979).

The FloEFD-calculated local Nusselt number dependences $Nu_x(Re_x)$ at the different incoming flow turbulence intensities with the semi-empirical dependences for air flows over flat plates (Pr=0.72) with laminar (4.4) and turbulent (4.5) boundary layers is shown in Fig, 7:

$$Nu_x = 0.332 \cdot Re_x^{1/2} Pr^{1/3}, \quad (4.4)$$

$$Nu_x = 0.032 \cdot Re_x^{0.8} Pr^{0.43}, \quad (4.5)$$

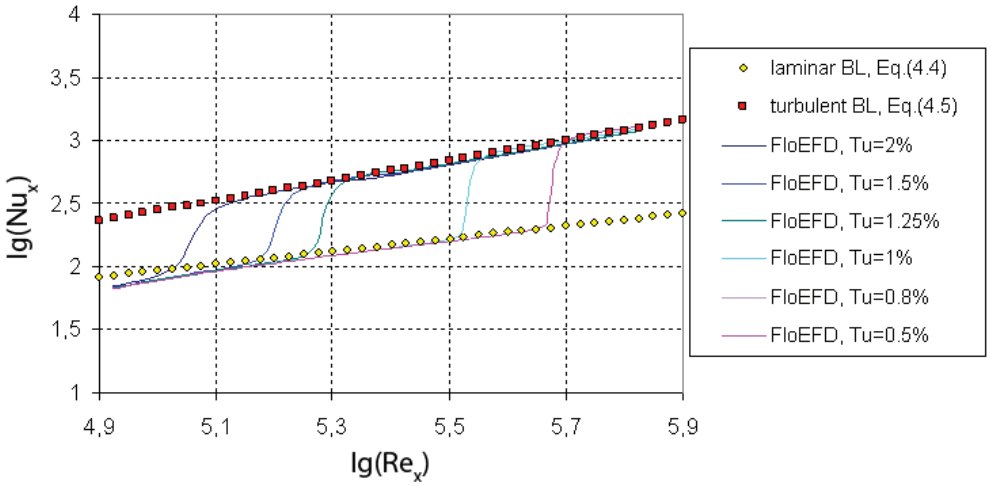

Fig.7. The local Nusselt number of air flow over a smooth flat plate vs. Re_x calculated with FloEFD and, for comparison, with the semi-empirical Eqs.(4.4) and (4.5) (Lienhard and Lienhard, 2004).

3.2 COUETTE FLOW BETWEEN TWO PARALLEL FLAT PLATES AT RE=3.4 X10^4

A classical plane flow is one between two parallel infinite flat plates spaced at a distance h from one another and moving at velocity U in opposite directions (Fig.8), so the flow Reynolds number, $\mathrm{Re} = \frac{\rho U h}{\mu = 3.4 \times 10^4}$.

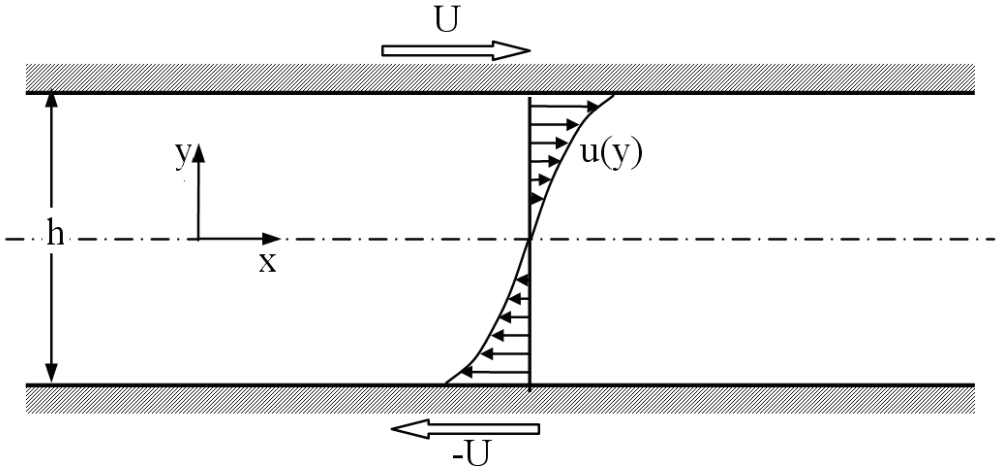

Fig.8. A turbulent Couette flow between two parallel plates moving in the opposite directions.

Dimensionless velocity profiles calculated within FloEFD for different computational meshes (10, 20, 40, 80 mesh cells across the channel) in comparison with experimental data (Schlichting, 1979) are shown in Fig.9.

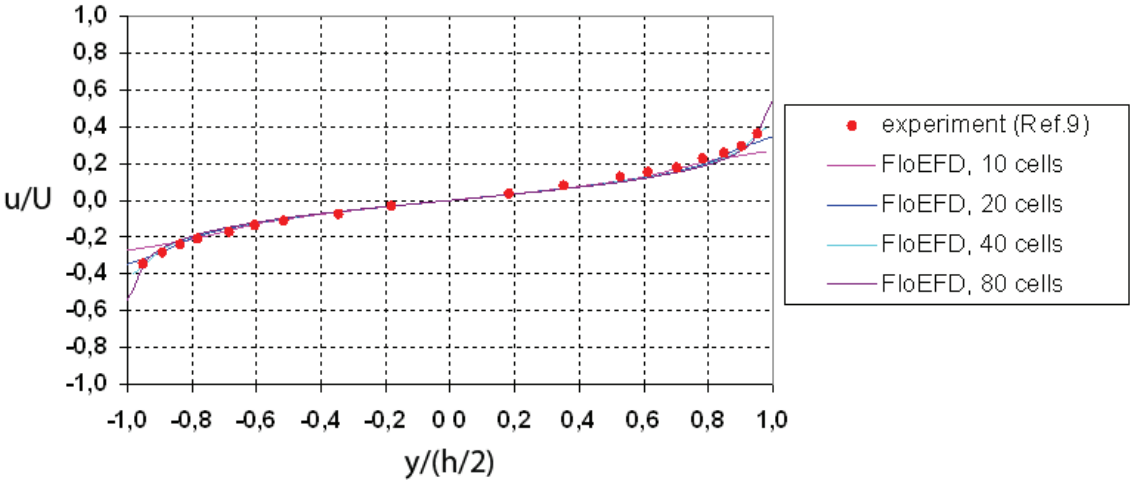

Fig.9. FloEFD-calculated dimensionless velocity profiles of turbulent Couette flow between two parallel plates moving in the opposite directions in comparison with the experimental data (Schlichting, 1979).

Good agreement between the FloEFD calculations with the experimental data is seen. y^+=75 for the 10 cells mesh, y^+=37.5 for the 20 cells mesh, y^+=19 for the 40 cells mesh, and y^+=9.5 for the 80 cells mesh showing how robust the solver is with coarse meshes.

3.3 FLOW OVER A BACKWARD-FACING STEP AT RE=5,000

Consider air flow in a rectangular channel having parallel walls (Hirsch, 1988), 1.0 m in length × 15.1 cm width × Y_0=10.1 cm in height as the inlet section, and an H=1.27 cm height backward-facing step on the bottom of the domain (Fig.10). Due to the channel's large aspect ratio (the tunnel-width to step-height ratio is equal to 12) three-dimensional effects in the flow separation region downstream of the backward-facing step are minimal, and due to the channel's small expansion ratio $(Y_0 + H)/Y_0$ = 1.125 the pressure gradient downstream of the sudden expansion is also at a minimum.

At a distance 4H upstream of the backward-facing step the inlet air flow has a velocity of 44.2 m/s, the atmospheric total pressure and temperature - this flow's Mach number is equal to 0.128 - and the fully turbulent boundary layer of 1.9 cm thickness provided by the high Reynolds number of 5,000 (based on the boundary layer momentum thickness).

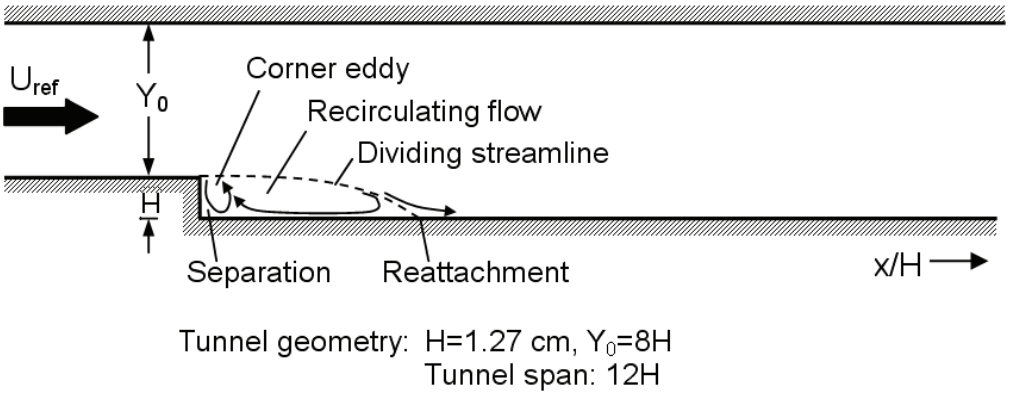

Fig.10. Flow in a rectangular channel with parallel walls and a backward-facing step on the bottom.

FloEFD calculations of this flow were performed on uniform computational meshes having 10, 20, and 40 cells per the step height (Fig.11).

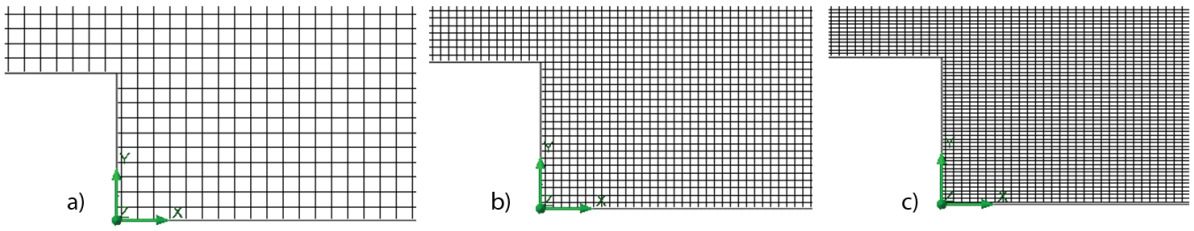

Fig.11. The FloEFD computational meshes of different density used: the number of cells traversing the step height: a) 10 cells, b) 20 cells, c) 40 cells.

FloEFD-calculated flow velocity profiles, wall friction downstream of the backward-facing step, and the separated flow reattachment's distance from the backward-facing step are presented in Figs.12 and 13 and in Table 1. In these calculations $y^+ = 0$ up to 54 in the computational mesh of 10 cells per step height, H, = 0 up to 27 at the computational mesh of 20 cells per H, and $y^+ = 0$ up to 13 at the computational mesh of 40 cells per H. Good convergence of these FloEFD calculation results with the computational mesh refinements chosen and good agreement of these results with the experimental data (Driver and Seegmiller 1985) and calculations (Wilcox 1994).

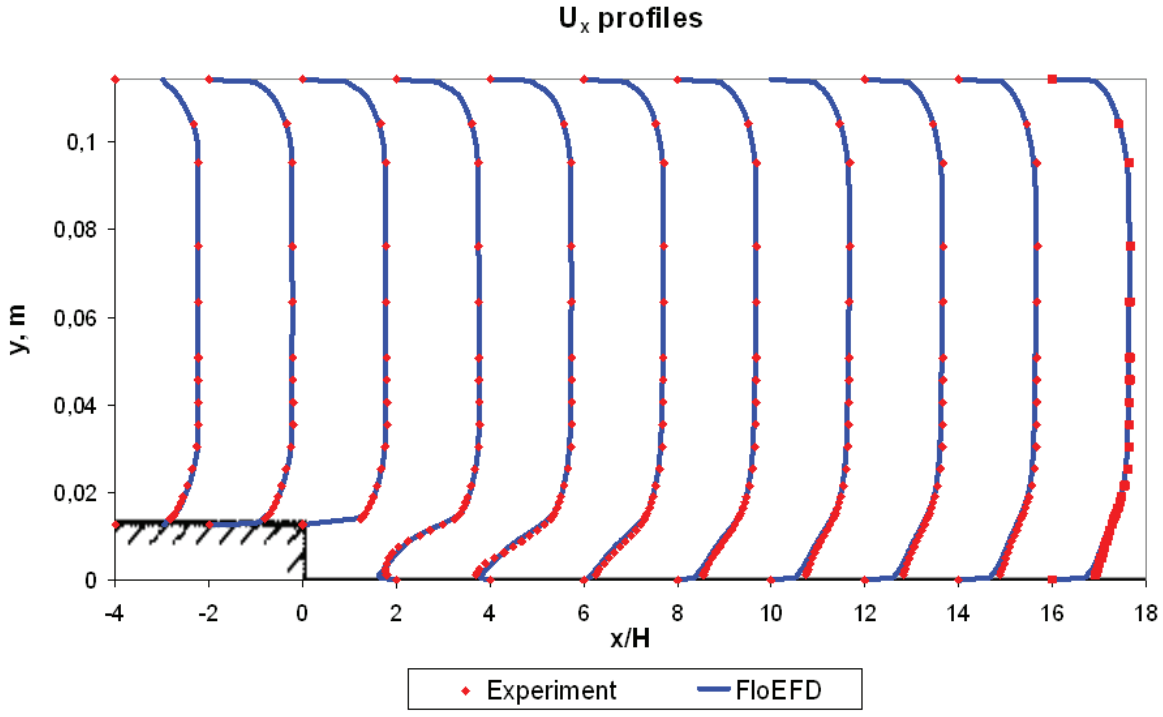

Fig.12. FloEFD-calculated flow velocity profiles obtained with the computational mesh of 10 cells per step height in comparison with experimental data (Driver and Seegmiller 1985)

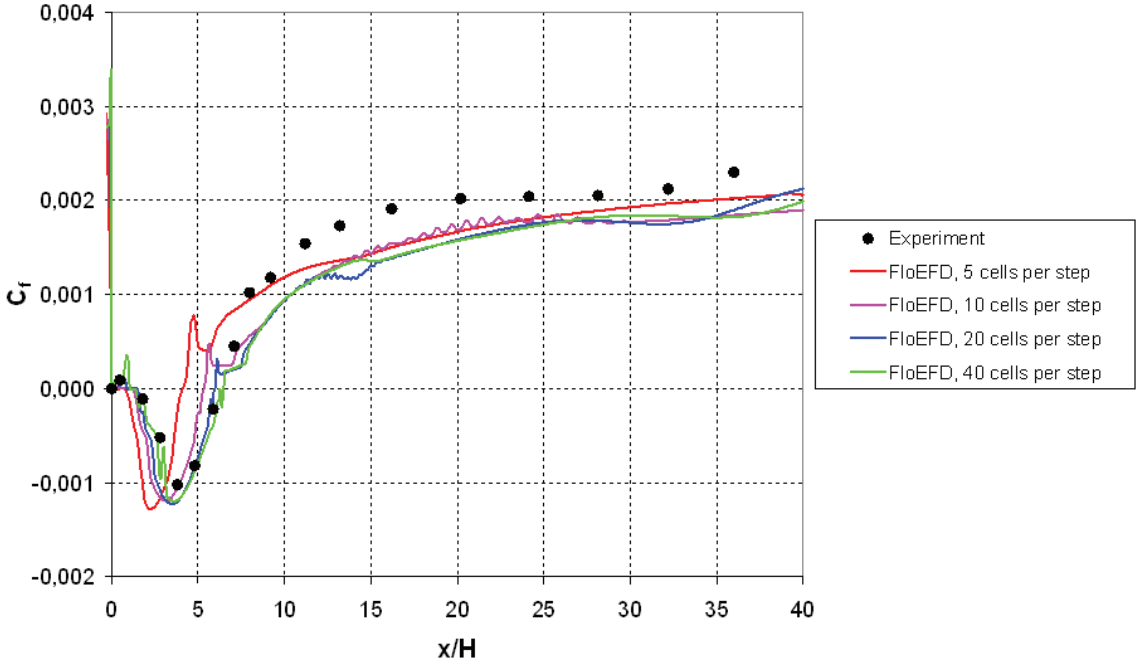

Fig.13. The FloEFD-calculated wall friction coefficient of the flow past the back step in comparison with experimental data (Driver and Seegmiller 1985).

	x/H	Deviation from experimental data (%)
Experiment (Driver and Seegmiller 1985)	6.2	0
FloEFD, 10 cells per H	5.37	-13
FloEFD, 20 cells per H	6.00	-3
FloEFD, 40 cells per H	6.27	1
Calculation with the k-ε model (Wilcox 1994)	5.2	-16
Calculation with the k-ω model (Wilcox 1994)	6.4	3

Table 1. FloEFD-calculated distance of the separated flow reattachment point downstream of the backward facing step in comparison with experimental data (Driver and Seegmiller 1985) and calculations (Wilcox 1994).

3.4 FLOW OVER A CYLINDER AT RE=3.7X10^5

Consider unsteady air flow over a circular cylinder at the incoming air flow velocity of 153 m/s under normal pressure and temperature at the cylinder-diameter-based Reynolds number of Re=3.7x10^5. FloEFD calculations were then carried out with computational mesh densities having 20, 40, and 80 cells per cylinder diameter. In all these calculations the thin-boundary-layer turbulence model was employed. The computational mesh and results for 20 cells per cylinder diameter is shown in Fig.14a. FloEFD-calculated velocity fields and an experimental shadowgraph (Driver and Seegmiller 1985) of real flow over a circular cylinder at nearly the same Reynolds number are shown in Fig.14.

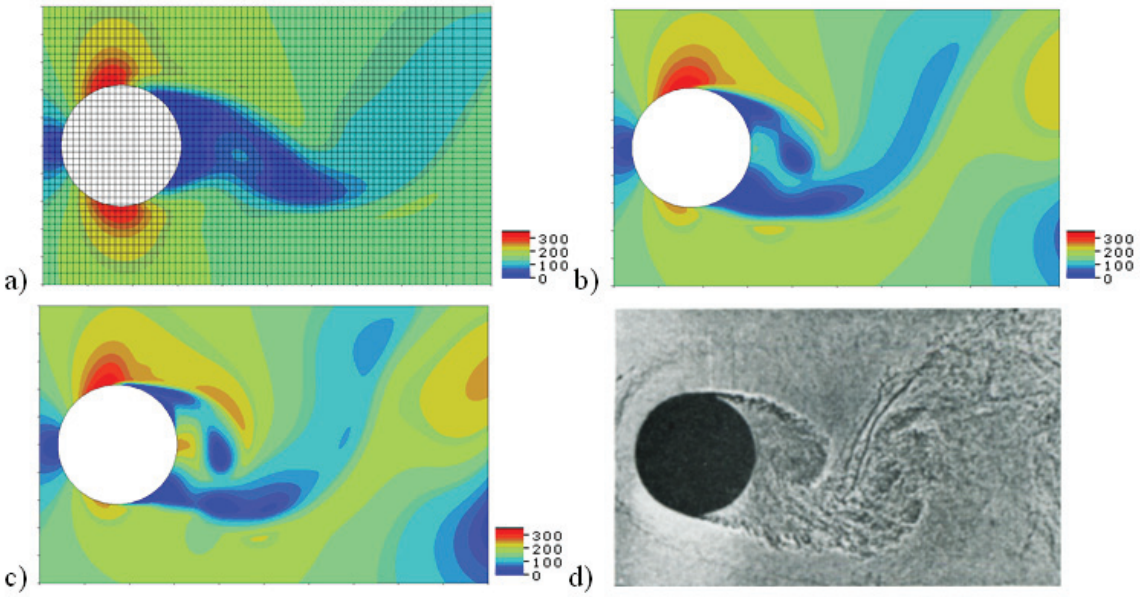

Fig.14. Predicted flow velocity fields over a circular cylinder, calculated with FloEFD for different computational meshes having a) 20 cells per diameter, b) 40 cells per diameter, c) 80 cells per diameter, and, d) similar real flow shadowgraph from Driver and Seegmiller (1985)

The drag coefficient, C_d, of the cylinder calculated with FloEFD for the different computational meshes in comparison with experimental data (Driver and Seegmiller 1985), as well as the corresponding y^+ values, are presented in Table 2.

Mesh Density (cells per cylinder diameter)	C_d	Deviation from the Ref.12 experimental data (%)	y^+_{max}
FloEFD, 20 cells per diameter	0.82	-18	650
FloEFD, 40 cells per diameter	0.95	-5	330
FloEFD, 80 cells per diameter	1.02	2	170
Experiment (Driver and Seegmiller 1985)	1.0	0	n/a

Table 2. Circular cylinder drag coefficients calculated with FloEFD in comparison with experimental data (Driver and Seegmiller 1985).

The FloEFD simulation predictions for varying computational mesh densities shows very good agreement with the experimental data from Driver and Seegmiller (1985).

3.5 FLOW OVER A GENERIC CAR BODY SHAPE (THE AHMED BODY)

A classical automotive external aerodynamics wind tunnel test case is the so-called "Ahmed Body" (Lienhart, Stoots and Becker 2000) which has a curved chamfered front end, box-like main body and sloping rear section. Using FloEFD an approaching air flow of 40 m/s on the generic model car body of 1,044 mm length, 389 mm width, and 288 mm height and mounted in a wind tunnel of 1,870 mm × 1,400 mm cross section at a 50 mm height above the floor on 4 stilts of 30 mm diameter was created - see Fig.16. The model car body's slanting rear section of 222 mm length was modeled with different (35° and 25°) slant angles.

In the experimental study flow had started to separate from the body's slanting surface at an angle of 30°. The flow's Reynolds number based on the body height and the incoming flow velocity is equal to Re = 7.68×10^5. FloEFD calculations were performed with a computational mesh of 209 cells in length, 58 cells in height, and 78 cells in width to resolve the car body (Fig.15).

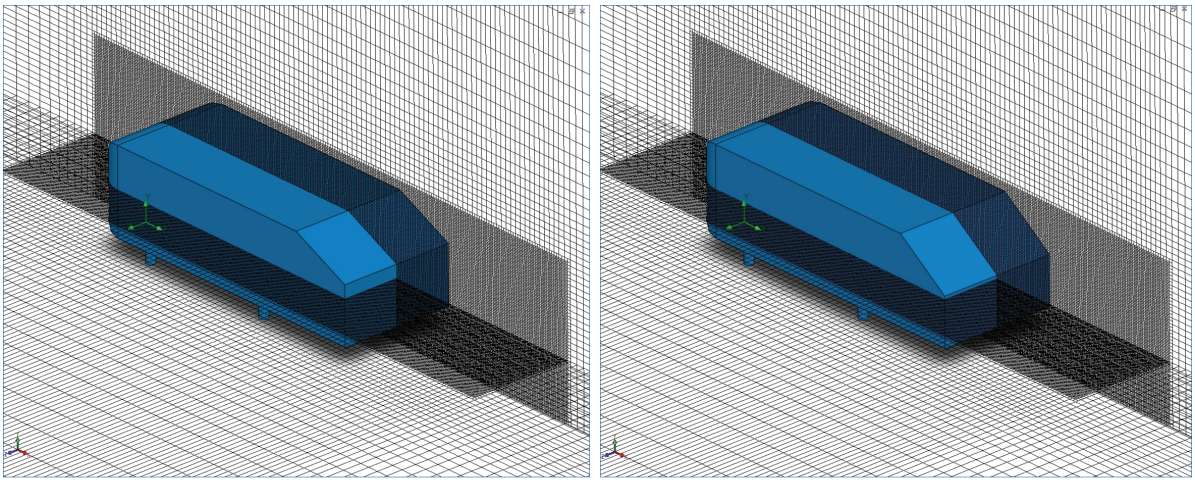

a) b)

Fig.15. The FloEFD computational mesh over the model car body: a) the 25° rear slant, b) the 35° rear slant.

FloEFD-calculated flow streamlines and velocity contours upstream, over, and downstream of the model car body are shown in Fig.16 for the two sloping rear slant angles. The FloEFD-calculated flow velocity profiles and body drag coefficients in comparison with the experimental ones (Lienhart, Stoots and Becker 2000) are shown in Fig.17 and Table 3. It can be seen from Figs.16 and 17 that in the FloEFD calculations the flow over the body is attached to the body's slanting rear surface if it has the 25° rear slant angle and separates from this surface if it has the 35° angle, and the calculated flow velocity profiles are close to the experimental ones. From Table 3 it is observed that the FloEFD-calculated body drag coefficients agree well with the experimental ones.

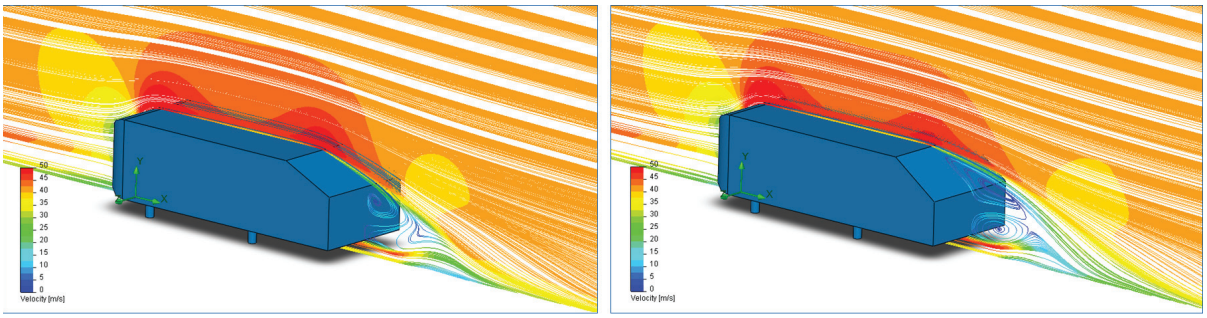

a) b)

Fig.16. FloEFD-calculated flow streamlines and velocity contours upstream, over, and downstream of the model car body: a) the 25° body slant, b) the 35° body slant.

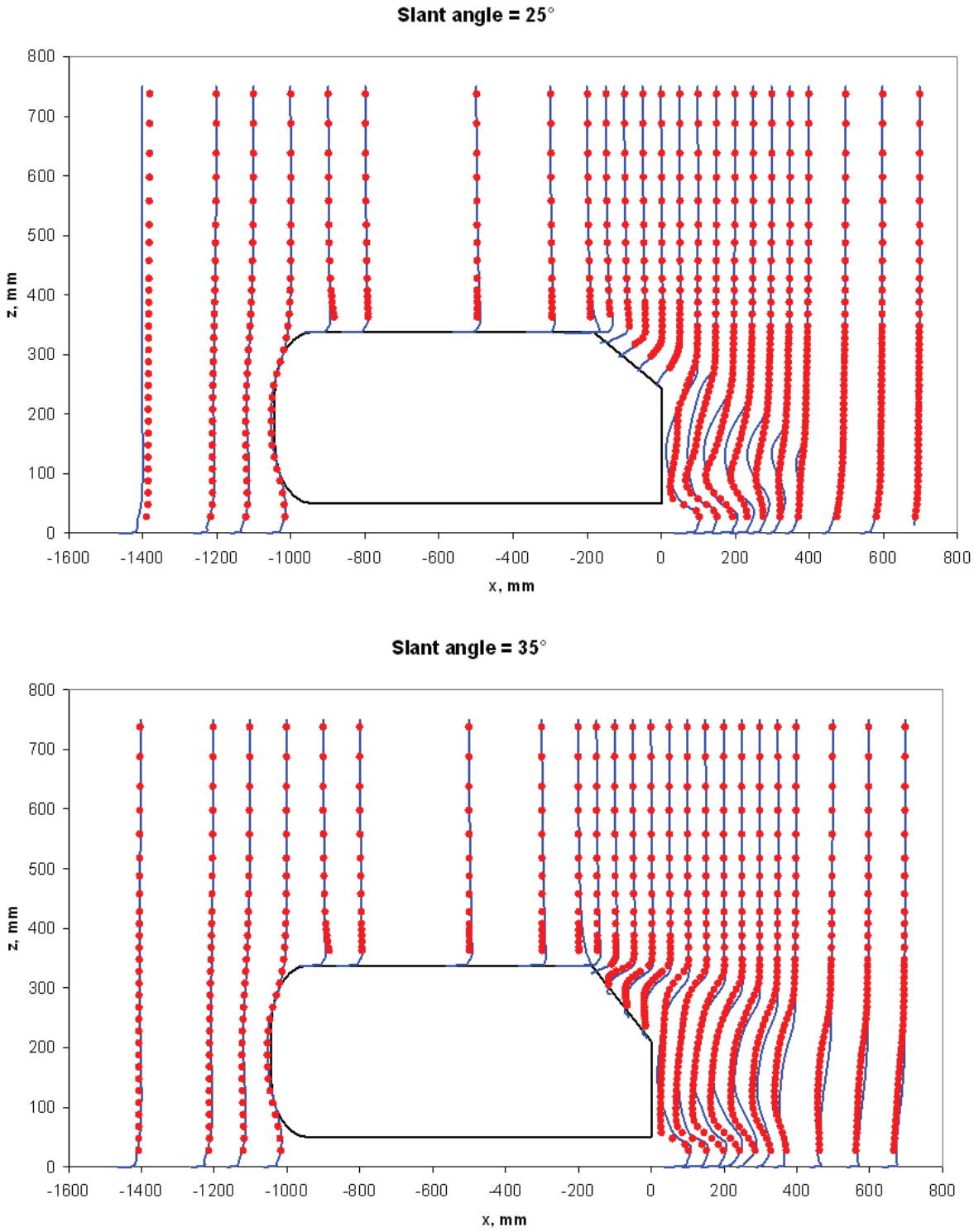

Fig.17. FloEFD-calculated flow velocity profiles in the body's symmetry plane in comparison with experimental data at the body's slant angles of 25° and 35° degrees: – FloEFD calculation, • experiment (Lienhart, Stoots and Becker 2000)

Ahmed body's slant angle	C_d, exp	C_d, FloEFD	Deviation from the Ref.13 experimental data (%)	y^+_{max} on the slanted surface
25°	0.298	0.284	-4.8	1401
35°	0.257	0.274	6.6	1402

Table 3. The model car body's drag coefficient calculated with FloEFD and obtained in Wind tunnel experiments (Lienhart, Stoots and Becker 2000)

CONCLUSIONS

The general purpose CAD-embedded CFD solver in the FloEFD software package from Mentor Graphics has been benchmarked against a wide range of CFD turbulence cases and its two equation modified k-ε turbulence model with its unique two-scale wall functions approach and immersed boundary Cartesian meshes leads to good predictions for spatial laminar, turbulent, and transitional flows over a range of compressible and anisotropic flows. Boundary layer resolution was good in all cases even though mesh densities were varied and coarse by traditional CFD approaches and the determination of wall friction and heat fluxes from the fluid flow to the wall interface over a wide range of Reynolds numbers was excellent.

REFERENCES

Driver, D.M. and Seegmiller, H.L., 1985. Features of a Reattaching Turbulent Shear Layer in Divergent Channel Flow. *AIAA Journal*, Vol. 23, p. 163.

Gavriliouk, V.N., Denisov, O.P., Nakonechny, V.P., Odintsov, E.V., Sergienko, A.A., Sobachkin, A.A., 1993. Numerical Simulation of Working Processes in Rocket Engine Combustion Chamber. *44th Congress of the international Astronautical Federation*, IAFF-93-S.2.463, October 16-22, Graz, Austria

Ginzburg, I. P., 1970. *Theory of Drag and Heat Transfer*. Leningrad, LGU (in Russian).

Griffiths, W.D., and Boysan, F., 1996. Computational fluid dynamics (CFD) and Empirical modelling of the performance of a number of cyclone samplers, *Journal of Aerosol Science*, Vol. 27, No. 2, pp. 281-304.

Hirsch, C. 1988. Numerical Computation of Internal and External Flows, Volume I*Fundamentals of Numerical Discretization*. New York: John Wiley & Sons.

Kalitzin, G., and Iaccarino, G., 2002. Turbulence Modeling in an Immersed-Boundary RANS method, *Center for Turbulence Research Annual Research Briefs*, Stanford University, California, pp. 415 - 426.

Lapin, Y.V., 1982. *Turbulent Boundary Layer in Supersonic Gas Flows*. Moscow, Nauka, (in Russian).

Lam, C.K.G. and Bremhorst, K.A., 1981. Modified Form of Model for Predicting Wall Turbulence. *ASME Journal of Fluids Engineering*, Vol.103, pp. 456-460.

Launder, B.E. and Spalding, D.B., 1972. *Lectures in Mathematical Models of Turbulence*. Academic Press, London, England.

Launder, B. E. and Spalding, D. B. The Numerical Computation of Turbulent Flows. *Computer Methods in Applied Mechanics and Engineering*, Vol.3, 1974, pp.269-289.

Lienhard IV, J.H. and Lienhard V, J.H., 2004. *A Heat Transfer Textbook*. 3rd ed., Cambridge, MA: Phlogiston Press.

Lienhart, H., Stoots, C., Becker, S., 2000. Flow and turbulence structures in the wake of a simplified car model (Ahmed model). *DGLR Fach Symp. der AG STAB*, Stuttgart University.

Mentor Graphics Corp., 2011. Advanced Immersed Boundary Cartesian Meshing Technology in FloEFD™.

Schlichting, H., 1959. *Entstehung der Turbulenz*. Berlin (in German).

Schlichting, H., 1979. *Boundary-Layer Theory*. McGraw-Hill, New York.

Van Driest, E.R., 1956. On Turbulent Flow Near a Wall. *Journal of the Aeronautical Science*, Vol. 23, No. 10, p.1007.

Wilcox, D.C., 1994. *Turbulence Modeling for CFD*. DCW industries.

	Nomenclature
u_i	i-th component of the fluid velocity vector
ρ	fluid density
k	turbulence energy
ε	dissipation rate of turbulence energy
μ	fluid viscosity
μ_t	fluid turbulent viscosity
τ_{ij}	*ij*-th component of the laminar stress tensor
τ_{ij}^R	*ij*-th component of the Reynolds stress tensor
Pr	the dimensionless Prandtl number
Pr_t	the dimensionless turbulent Prandtl number
C_P	fluid specific heat capacity under constant pressure
T	temperature
x_i	*i*-th component of the Cartesian coordinate system
n_i	*i*-th component of the normal to the wall in the fluid region
y	distance from the wall along the normal to it
y^+	dimensionless distance from the wall along the normal to it
τ_w	wall shear stress
q_w	heat flux from the wall to the fluid
κ	the Karman factor
A_v	the Van Driest dumping factor
k_s	equivalent sand roughness height
δ	boundary layer thickness calculated by the integral method
u^e	fluid velocity at the fluid boundary of the boundary layer
τ_w^e	wall friction calculated by the integral method
q_w^e	heat flux from the wall to the fluid, calculated by the integral method

	Subscripts
i, j, k	directions of the Cartesian coordinate system
w	at the wall

Corporate Headquarters
Mentor Graphics Corporation
8005 SW Boeckman Road
Wilsonville, OR 97070-7777
Phone: 503.685.7000
Fax: 503.685.1204

Sales and Product Information
Phone: 800.547.3000
sales_info@mentor.com

Visit www.mentor.com/company/office_locations/ for the list of Mechanical Analysis Division Offices

MGC 02-11 TECH9670-w